Atmos. Chem. Phys. Discuss., 11, 28587–28626, 2011
www.atmos-chem-phys-discuss.net/11/28587/2011/
doi:10.5194/acpd-11-28587-2011

Atmospheric Chemistry and Physics Discussions

Long-term simulations (2001–2006) of biomass burning and mineral dust optical properties over West Africa: comparisons with new satellite retrievals

F. Malavelle[1,2], **M. Mallet**[1,2], **V. Pont**[1,2], **C. Liousse**[1,2], **and F. Solmon**[3]

[1]Université de Toulouse, UMR5560, UPS, LA (Laboratoire d'Aérologie), 14 avenue Edouard Belin, 31400 Toulouse, France
[2]CNRS, LA (Laboratoire d'Aérologie), 31400 Toulouse, France
[3]International Centre for Theoretical Physics, Trieste, ESP (Earth System Physics), Italy

Received: 8 September 2011 – Accepted: 20 September 2011 – Published: 25 October 2011

Correspondence to: F. Malavelle (malf@aero.obs-mip.fr)

Published by Copernicus Publications on behalf of the European Geosciences Union.

Abstract

The West African region is characterized by large concentrations of smoke and biomass burning aerosols, which could significantly modify the regional radiative budget and the hydrological cycle. Here, we propose long-term (2001–2006) RegCM simulations of aerosol optical properties over West Africa together with their spectral dependences. Results of simulations are evaluated at local and regional scale by using surface network (AERONET/PHOTON) and remote sensing observations (MODIS, MISR, OMI) especially during the dry season, December-January-February, DJF. New original satellite retrievals are tested and compared to RegCM simulations. Concerning AOD, we obtain values in agreement with AERONET/PHOTON observations at the local scale but some differences clearly appear between simulated AOD and regional MISR, OMI and MODIS view, especially over (1) the central Africa and (2) the gulf of Guinea during DJF. Concerning simulated SSA (for visible wavelengths), our results display (1) comparable values with level 2 AERONET/PHOTON local observations together with (2) non negligible differences with satellite (MODIS Deep blue, OMI and MISR products) observations. In most cases, satellite SSA is found to be higher than those simulated by RegCM and retrieved through AERONET/PHOTON network. In parallel, we also note significant differences on retrieved SSA from each satellite (OMI, MISR, MODIS Deep Blue) remote sensing techniques over this specific region. Finally, our work highlights that the spectral dependence of aerosol optical properties is a useful parameter to adapt so that modeled simulations should be be better evaluated and constrained.

1 Introduction

Africa is the world's largest source of biomass burning (BB) and mineral dust aerosols (Prospero and Lamb, 2003; van der Werf et al., 2006). In the arid northern part, atmospheric aerosol loads are largely influenced by large amounts of mineral dust

ACPD
11, 28587–28626, 2011

aerosols. These mineral dust particles are emitted continuously during the year and are able to modulate the radiative balance both at local (Slingo et al., 2009) and regional scales (Grini et al., 2006; Solmon et al., 2008; Milton et al., 2008; Mallet et al., 2009; Cavazos et al., 2009). Intense events of dust uplift that regularly occur, have ever been well documented (e.g. Myhre et al., 2003; Slingo et al., 2006; Heinold et al., 2007; Tulet et al., 2008; Crumeyrolle et al., 2011). Many studies account for the dusty outflow and its ageing from the West Africa towards Atlantic Ocean (Schepanski et al., 2009; Dall'Osto et al., 2010).

In the western part of the continent, the atmosphere is also heavily loaded by carbonaceous aerosols from anthropogenic and biomass burning sources (Liousse et al., 1996; Cooke et al., 1999; Junker and Liousse, 2008; Liousse et al., 2010). Biomass burning emissions are likely to be the dominant contributor among these sources of carbonaceous aerosols in the region (Liousse et al., 2004; Myhre et al., 2008). These follow a seasonal cycle with intense fire events during dry season (December to February) and lowest ones during wet season (Roy et al., 2008). Remote sensing observations of the fine mode aerosol optical thickness (AOT) show that biomass burning aerosols are a major contributor to the total bulk AOT in West Africa during dry season (Tanré et al., 2001).

At present, most of 3-D numerical exercises (Yoshioka et al., 2007; Solmon et al., 2008; Konare et al., 2008; Sud et al., 2009; Lau et al., 2009) have been mainly focused on the effect of dust aerosols on the West Africa regional radiative budget through their direct and semi-direct radiative effects. The associated feedbacks due to dust particles on the hydrological cycle and on the atmospheric dynamic of the West African monsoon have been also estimated in recent studies (Lau et al., 2009; Huang et al., 2009a, b; Klüser and Holzer-Popp, 2010; Perlwitz and Miller, 2010; Zhao et al., 2011). As the West African atmosphere is also heavily loaded by smoke aerosols resulting from the incomplete combustion of fossil fuels, biofuels (domestic fire) and biomass burning (Liousse et al., 1996; Cooke et al., 1999; Junker and Liousse, 2008; Liousse et al., 2010) and due to the ability of such aerosols to significantly modify the radiative

ACPD
11, 28587–28626, 2011

budget (Haywood et al., 2008; Johnson et al., 2008b; Mallet et al., 2008), it appears necessary to investigate the possible impact of the total bulk aerosols on the regional climate, including smoke particles.

Such a study firstly requires controlling the total bulk optical properties before investigating the possible climatic feedbacks. Indeed and contrary to mineral dust particles (i.e., moderate absorbing particles), smoke aerosols are able to strongly absorb (Johnson et al., 2008b) solar radiations and consequently modify the radiative heating profiles of the atmosphere. In that sense, this critical optical property (absorbing efficiency), need to be rigorously evaluated. In that frame and thanks to new original satellite retrievals (MODIS Deep blue, MISR and OMI products), together with surface remote sensing techniques (AERONET/PHOTON inversions), we test our results of simulations in terms of Aerosol Optical thickness (AOT), Absorption Aerosol Optical Thickness (AAOT) and Single Scattering Albedo (SSA). Furthermore, the spectral dependence of optical properties is also investigated. This work represents, to our knowledge, the first inter-comparison study using these new aerosol satellite products (at different wavelengths) and 3-D regional modelling outputs.

Based on dust parameterizations of Zakey et al. (2006) and Solmon et al. (2008), we performed, over the period 2001–2006, aerosol optical properties simulations over West Africa. As mentioned above, in addition to dust aerosols, biomass burnings and fossil fuels carbonaceous aerosols are also considered in this modelling exercise. Thus, the seasonal variability of bulk aerosol optical properties are evaluated thanks to outputs not only fitted to AERONET products but also to those supplied by MODIS Deep Blue, MISR or OMI satellites. Our study enables to check the variability of the atmospheric aerosol loading and absorbing optical properties at regional scale.

The paper is structured as follows. In Sect. 2, we describe the methodology and data used in this work. The modelling assumptions regarding aerosols and RegCM setups are described in Sect. 2.1. The observations used for comparisons with model outputs are detailed in Sects. 2.2 and 2.3. The results are discussed in Sect. 3. We first compare the modelled results to AERONET/PHOTON ground-based network in

ACPD
11, 28587–28626, 2011

Sect. 3.1. The regional comparisons of simulated and retrieved AOT and SSA over land and ocean are discussed in Sect. 3.2. The spectral dependence of AOT and AAOT are discussed in Sect. 3.3. Concluding remarks and perspectives are summarized in Sect. 4.

2 Methodology and data

We use in this work the RegCM3 model developed at the Abdus Salam International Centre of Theoretical Physics (ICTP) (Giorgi and Mearns, 1999; Pal et al., 2007) to investigate the spatial and temporal variability of aerosol optical properties in West Africa. In these simulations, we consider dust aerosols emitted from the erosion of arid soils, and carbonaceous and sulphate aerosols resulting from Biomass Burning (BB), combustion of Bio-Fuel (BF) together with Fossil Fuel (FF). We simulate the period spanning from January 2001 to January 2007.

In this study, we focus our analyses on aerosols fields, in particular the aerosol absorption property. In fact, aerosol absorption (typically expressed in terms of aerosol single scattering albedo) is one of the largest contributor to the total uncertainty in aerosol direct radiative forcing (McComiskey et al., 2008). At present, most comparisons between models and satellite have been conducted with AOT. In order to evaluate the accuracy of RegCM simulations, we compare modeled aerosols optical properties outputs to data retrieved from local remote sensing observations (AERONET/PHOTON ground-based network) together with those obtained from current generation of Earth Observatory System and A-train spaceborne instruments, providing a regional picture conversely to local stations. To strengthen our comparative approach at regional scale we consider aerosols retrievals from three different sensors including the Multi-angle Imaging SpectroRadiometer (MISR), the Moderate Resolution Imaging Spectroradiometer (MODIS) and the Ozone Monitoring Instrument (OMI). All these sensors not only offer the advantage of estimating the aerosol optical thickness, but give also estimation of aerosols absorption properties through the AAOT and SSA. Future promising

ACPD
11, 28587–28626, 2011

developments are conducted using PARASOL (Dubovik et al., 2011) but the data are not available at present. Besides, another benefit of these products is that they provide near-global daily distribution of aerosol optical properties at multiple wavelengths. This allows to investigate the spectral dependence of aerosol optical properties. The following subsections shortly describe the model setups and the different useful measurements.

2.1 The RegCM3 Model, configuration and aerosol optical properties

The RegCM modeled domain covers Western Africa (~20° W–40° E, 5° S–35° N), with a 45 km horizontal resolution on 18 hydrostatic sigma levels in the vertical. The model is driven at boundaries by the ERA Intererim reanalysis (Simmons et al., 2007). Model setup and parameterizations are similar to that described in Malavelle et al. (2011). We briefly remind here some of the aerosol assumptions considered in this study. First, dust aerosol emissions are prescribed by an online dynamical scheme (Zakey et al., 2006) which follows the saltation (horizontal flux) and sandblasting (vertical flux) parameterizations from Marticorena and Bergametti (1995) and Alfaro and Gomes (2001), respectively. The dust aerosols are represented by four tracers binned into (0.1–1.0 µm; 1.0–2.5 µm; 2.5–5.0 µm; 5.0–20 µm) in diameter. Secondly, emissions of carbonaceous and sulphate aerosols are prescribed by inventories dataset. The bbAMMA inventories are based on the Système Probatoire d'Observation de la Terre (SPOT) vegetation burnt area products (Michel et al., 2005; Liousse et al., 2010). Anthropogenic (FF and BF) aerosol emissions are based on the Junker and Liousse (2008) inventory. Carbonaceous aerosols are represented by two tracers BC and OC standing for Black carbon and Organic Carbon.

The RegCM model enables to follow the evolution of the mass concentration of externally mixed aerosol tracers. The AOT is estimated by multiplying the mass extinction efficiency (the extinction normalized by the mass, Kext in $m^2\,g^{-1}$), to the prognostic mass of each tracer and is then vertically integrated. The spectral dependence of AOT provides also additional information and enables us to distinguish between fine

ACPD
11, 28587–28626, 2011

anthropogenic aerosols (e.g. carbonaceous aerosols from pollution and/or combustion) and natural particles (mainly dominated by coarse aerosols such as mineral dust or sea salt). The spectral dependence of AOT can be represented in term of AOT Angstrom Exponent (AEAOT) expressed as:

$$\mathrm{AEAOT}_{\lambda_1-\lambda_2} = -\frac{\mathrm{LOG}(\mathrm{AOT}_{\lambda_1}/\mathrm{AOT}_{\lambda_2})}{\mathrm{LOG}(\lambda_1/\lambda_2)} \quad (1)$$

Where λ_1 and λ_2 are the radiation wavelengths. For typical aerosols mixture observed in West Africa, AEAOT between 440 and 870 nm is lower than 0.5 when coarse mineral dust dominate the mixture while it is above 1 when fine smoke particles are present. The AOT can be discriminated in the sum of absorption AOT and scattering AOT corresponding to the two pathways of the light extinction. In a similar way to AEAOT we can define an AE for SSA (AESSA) and AE for AAOT (AEAAOT) that better help to identify the different type of aerosols and to make comparisons with observed data. Indeed, biomass burning and dust aerosols spectral absorption have different slopes. Russell et al. (2010) reported AEAAOT encompassed between 2 and 3 for dust aerosols, whereas values around 1.45 for biomass burning aerosols.

As mentioned in Malavelle et al. (2011), we took advantage of AMMA-SOP0 in-situ observations to update biomass burning BC and OC tracers optical properties parameterizations used in RegCM3. These optical calculations are based on the measured mass size distributions of aged smoke aerosols obtained from Dekati impactor measurements at Djougou (Northern Benin) during AMMA-SOP0 (Pont et al., 2009). As biomass burning aerosols may exhibit varying optical properties depending on the weather conditions, the combustion phase and the type of vegetation burnt (Reid et al., 2005) it was worth considering specific optical properties of the biomass burning aerosols over this region. As an example, the low dry smoke SSA (~0.81 at 550 nm, Johnson et al., 2008b) estimated during AMMA-SOP0 differs from the one obtained during SAFARI 2000 over South-Africa (SSA in the range 0.83–0.92 for aged biomass burning aerosol and a mean value of 0.88 at 550 nm, Haywood et al., 2003b).

ACPD
11, 28587–28626, 2011

Based on the mass ratio at emission between OC and BC in bbAMMA inventories and the work of Pont et al. (2009), we estimate mean mass extinction efficiency (K_{ext}) for biomass burning aerosols equal to 6.35 $m^2\,g^{-1}$ (at 500 nm). This value is found to be consistent with the one (5.8 $m^2\,g^{-1}$ at 550 nm) reported by Johnson et al. (2008b) during DABEX campaign in West Africa. As previously noted, such values slightly differ to the one (5.0 $m^2\,g^{-1}$ at 550 nm) reported by Haywood et al. (2003b) during SAFARI 2000 (using identical techniques and corrections).

The optical properties (between 440 and 675 nm) of BC,OC and DUST tracers used as inputs in radiative transfer modelling (K_{ext}, SSA and *g* the asymmetry parameter) are summarized in Table 1. The optical properties for dust aerosols are similar to those detailed by Solmon et al. (2008).

2.2 Ground-based AERONET/PHOTON network

AERONET/PHOTON is the federated network of data archive system and ground based sun-photometers routinely performing sun and sky radiance measurements to retrieve global aerosols properties (Holben et al., 1998). Along with AOT observations, AERONET/PHOTON aerosol retrieval algorithm delivers the complete set of aerosol parameters (retrieved over the whole atmospheric column) including volume size distribution, single scattering albedo, refractive index and asymmetry parameter (and their spectral dependence between 440 nm and 1020 nm, Dubovik et al., 2002). In this study, we focus our comparisons between the simulated RegCM3 AOT and SSA and the AERONET/PHOTON level 2.0 (cloud-screened and qualityassured) sky radiance data and level 2.0 sky radiance inversions (at 440 and 675 nm). Estimates of the uncertainties for AOT are 0.015 at wavelengths greater than 440 nm while uncertainty in terms of SSA is estimated to be 0.03 for AOT >0.2 (0.07 for AOT <0.2) (Dubovik et al., 2000). Five sites of West Africa (Djougou (Benin), Banizoumbou (Niger), Ilorin (Nigeria), Agoufou (Mali) and Capo Verde (Senegal)) are selected as they present a long-time period of observations that fits well to the period of simulation. In addition, the geographic positions of the sites allow us to consider different aerosol mixtures.

ACPD
11, 28587–28626, 2011

Indeed, the sites located in the Sahelian belt (South of Saharan desert <15° N) are close to the BB sources during wintertime while Capo Verde is usually dominated by dust particles within the African dust outflow.

2.3 Satellite observations of aerosols properties

To evaluate the modeled outputs at regional scale, spatialized satellite data are used. As mentioned previously, we used in this work the MODIS, MISR and OMI sensors that deliver aerosol absorbing properties products.

2.3.1 MODIS

MODIS is a 36-channel spectrometer (0.412–14.2 µm) with daily global coverage. MODIS observes detailed aerosol properties with spatial resolution ranging from 0.25–1 km through measurement of spectral radiances. The MODIS retrieval algorithm (hereafter referred as the MODIS standard algorithm) uses two separate ways to derive aerosol characteristics, with one over ocean (Tanré et al., 1997) and one over land based on the dark target approach (Kaufman et al., 1997). In parallel to the aerosol retrievals classically conducted over the dark vegetation, the Deep Blue aerosol algorithm (Hsu et al., 2004) was developed to infer aerosol properties over highly reflective surfaces, using the blue channels radiance measurements. When the retrieval algorithm successfully identifies the aerosols scene as "Fine or Mixed Aerosols", the corresponding values of AOT and Angström exponent are reported. For "dust-dominant" cases, the values of single scattering albedo are retrieved in addition to the AOT and the Angström exponent.

In this study, we use the daily level-3 MYD08 collection 5.1 product from Aqua MODIS. The MODIS AOT maps presented are composite of the standard Aqua-MODIS retrieval together with Deep Blue retrieval. AOT uncertainties over vegetated land by MODIS standard retrieval against AERONET data is $\pm 0.05 \pm 0.15 \times \tau$, where τ is the AOT (respectively $\pm 0.03 \pm 0.05 \times \tau$ over ocean) (Remer et al., 2005). Hsu et al. (2006)

ACPD
11, 28587–28626, 2011

show that the values of satellite-retrieved AOT at 490 nm with Deep Blue algorithm are generally within a range of 20–30 % of AERONET/PHOTON AOT over East Asia.

2.3.2 MISR

MISR onboard the NASA EOS Terra (passing time 10:30 a.m. at equator) provides estimates of AOT and SSA using four different band channels (centred at 446, 558, 672, and 867 nm) and nine different viewing angles (nadir plus 26.1°, 45.6°, 60.0°, and 70.5° in the forward and aftward directions along the spacecraft track) with a spatial resolution of 275 m to 1 km. The key advantage of MISR measurements approach is the use of different geometry views allowing MISR to retrieve aerosol properties without any limitations due to surface reflectance (Diner et al., 1998) or sunglint. However, the narrow swath of the instrument (~360 km wide swath) only permits to obtain a global coverage once in nine days (at equator). It should be noted that there are different sampling rates between MISR and MODIS sensors, which may affect monthly means particularly over cloudy regions. We consider here the daily level-3 data MIL3-DAE products version F15-0031. A global comparison of MISR and AERONET AOT shows that overall about 70 % to 75 % of MISR AOT retrievals fall within 0.05 (or 20 % of τ_{AERONET}) of the paired validation data from the AERONET/PHOTON, and about 50 % to 55 % are within 0.03 or (10 % of τ_{AERONET}).

2.3.3 OMI

The Ozone Monitoring Instrument (OMI) operating since October 2004 onboard of the EOS Aura satellite is a spectrometer with high spectral resolution (Levelt et al., 2006). OMI has a swath width of 2600 km and offers nearly daily global coverage with a spatial resolution for the UV-2 and VIS (UV-1) channels reaching 13×24(48) km^2 at nadir. Because of the relatively large resolution of the OMI observations, the major factor affecting the quality of aerosol products is sub-pixel cloud contamination. In parallel, one can mention that OMI can detect bulk aerosols signal from its measurements in the UV

ACPD
11, 28587–28626, 2011

spectral range also in cloudy scenes. However, in this study we use the data from the OMAERUV0v003 product containing retrievals for clear sky conditions from OMI near-UV algorithm (Torres et al., 2007). The near UV method of aerosol characterization uses space measurements at two channels in the near UV to detect aerosol absorption. This algorithm provides a variety of aerosol radiative properties, such as aerosol index, AOT, AAOT and SSA. In general OMI Near-UV retrievals are more reliable over land than over water surfaces. The near-UV retrieval method is particularly sensitive to carbonaceous and mineral dust aerosols. OMI measurements in Near-UV also depend on the height of the aerosol layer above the ground (Torres et al., 1998). In that frame, the OMI near-UV algorithm sensitivity is largest for elevated (at least 2 km above the surface) aerosol layers, and decreases rapidly with aerosol layer height. It should be noted that recent modifications have been conducted by Jethva and Torres (2011) to improve SSA retrievals from OMI.

3 Results and discussions

3.1 Comparison of aerosols optical properties at local scale with AERONET/PHOTON data

3.1.1 AOT

RegCM is designed to conduct long-term climatic simulations including the possibility to take into account the interaction between particles and SW and LW radiations. In order to evaluate if the model correctly estimates the aerosol loading at such timescale, we first compare (Table 2) the seasonal average (DJF and JJA) AOT at 440 nm and 675 nm simulated by RegCM with AERONET/PHOTON data. We complete the Table 2 with MODIS (DEEP BLUE algorithm only) and MISR retrieved AOT in the pixel close to the selected stations.

ACPD
11, 28587–28626, 2011

During DJF, simulated AOT at Capo Verde, Banizoumbou and Agoufou (at 440 and 675 nm) are within 20 % of AERONET/PHOTON values, while at Ilorin and Djougou, the model significantly underestimates the AERONET/PHOTON observations, possibly due to an inaccurate representation of the transport of BB aerosols in the upper atmospheric layers. Similar results are obtained when comparing simulated AOT with those obtained from satellite remote sensing. Indeed, comparisons indicate a relatively good agreement between the model and observations in case of "dusty" sites (Table 2) such as Capo Verde (RegCM AOT ~0.22, MISR AOT ~0.30, MODIS Deep blue AOT ~0.20 at 440 nm). In contrast, large differences are observed for site highly influenced by smoke aerosols, such as Djougou (RegCM AOT ~0.37, MISR AOT ~0.53, MODIS Deep Blue AOT ~0.66, at 440 nm). During DJF, the predominance of BB aerosols in the mixing appears clearly in the AERONET/PHOTON AEAOT showing the highest values at Djougou and Ilorin. In contrast, the Agoufou, Banizoumbou and Capo Verde sites display averaged AEAOT lower than 0.5, due to the significant presence of coarse dust aerosols.

During JJA, when dust aerosols are the main compounds remaining in the West African atmosphere, we observe that the RegCM model performs better than during DJF. On average and over the five sites, RegCM errors on AOT, compared to AERONET/PHOTON observations, is about 44 % and 20 % (at 440 and 675 nm, respectively) during DJF, while in JJA the error is respectively about 36 % and 1 %. Comparisons of simulated AOT with satellite observations reveal also a better agreement during this season, except at Banizoumbou where large difference remain (RegCM AOT ~0.35, MISR AOT ~0.59, MODIS Deep Blue AOT ~0.70, at 440 nm).

In parallel to the magnitude of AOT, we also focus our investigations on the spectral dependence of AOT, which represents a critical property concerning the direct effect of particles. First, we can mention that when aerosols are composed by dust and BB particles (in DJF), simulated AEAOT are higher than in the case of a pure dust (JJA) accordingly to the presence of fine BB aerosols (see Table 2). Nevertheless, we can note that RegCM is misrepresenting the AEAOT (calculated between 440 and 675 nm)

ACPD
11, 28587–28626, 2011

both in DJF and JJA for the two types of particles. We can observe that RegCM AEAOT is negative for each site with lower values during the dry season. This reversed spectral dependence is due to the optical properties assigned to the fine mode (first bin) of dust aerosols, with a mass extinction efficiency of 1.89 $m^2 g^{-1}$ and 2.93 $m^2 g^{-1}$ at 440 nm and 675 nm, respectively (see Table 1). This reversed spectral dependency of the extinction for the fine dust aerosols is not realistic and explains the simulated negative AEAOT values. In that sense, future works are scheduled for updating the spectral dependence of mineral dust in RegCM by using recent AMMA observations (McConnell et al., 2010).

3.1.2 SSA

The RegCM simulated SSA and the SSA retrieved from AERONET/PHOTON and (MISR and MODIS Deep Blue) satellite inversions (at 440 nm and 675 nm) are also reported in Table 2.

During the DJF season, RegCM SSA values are shown to be in good agreement with AERONET/PHOTON retrievals. Simulated SSA falls in the range of ~±0.02 of AERONET/PHOTON SSA values except at Capo Verde where RegCM SSA is equal to 0.902 and 0.950 (at 440 and 675 nm) while AERONET/PHOTON is 0.858 and 0.897 (±0.03). This may result from a lack of long range transport of elevated biomass burning aerosols from the sources region in the model and/or, a lack of biomass sources in the western part of the domain. We observe also, both in AERONET/PHOTON and simulated RegCM SSA, a well marked seasonal cycle with the lowest SSA values in DJF and the highest in JJA, in agreement with the seasonal cycle of biomass burning emission. We note also that, during JJA, SSA values are largely dominated by dust aerosols, with an averaged AERONET/PHOTON SSA of 0.91±0.03 (at 440 nm).

Concerning the new aerosol SSA retrieved products, our study seems to indicate that MISR SSA values are higher than RegCM and AERONET/PHOTON data especially during DJF, while the difference is lower during JJA. In most of cases, the MISR SSA is about 1 (at 440 and 675 nm) for all the sites studied (Table 4.3). This

ACPD
11, 28587–28626, 2011

systematic overestimation of SSA in MISR products have already been reported in Kahn et al. (2010). In the same way, the MODIS/Deep Blue SSA products are higher than RegCM and AERONET/PHOTON SSA and do not show a marked seasonal variation. For most of cases, MODIS retrievals indicate intermediate SSA values comprised between AERONET/PHOTON and MISR observations. We recall here, that MODIS Deep Blue product SSA values over bright surfaces are only reported for dust dominant pixels. Consequently, if there is significant amount of biomass burning smoke in the atmosphere during the dry season (DJF), the uncertainty in the retrieved SSA becomes larger (Hsu et al., 2006).

3.2 Comparison of aerosol optical properties at regional scale

Figure 1 presents the averaged AOT for DJF and JJA estimated by RegCM (at 500 nm), MODIS composite (at 550 nm), MISR (at 555 nm) and OMI (at 500 nm) sensors.

3.2.1 AOT observed over land

Several areas of interest can be identified over lands. First and during the dry season it can be seen (Fig. 1) in satellite observations that maximum of AOT are usually found over the Bodélé depression (Chad). MISR AOT obtained over the Bodélé depression is lower than MODIS and OMI observations. The narrow viewing swath of MISR (360 km compared to 2600 km and 2330 km for OMI and MODIS) can fail daily storms events explaining underestimations in the average aggregate (Ahn et al., 2008). Figure 1 also clearly shows that RegCM underestimates (AOT ~0.45-0.50 at 500 nm) the Bodélé sources due to underestimation of local wind as already reported in Todd et al. (2008). In parallel, RegCM performs well over the Northern part of the West African continent but overestimates the AOT over Mauritanian and Mali, compared to MISR and MODIS Deep Blue retrievals.

The central African region is also characterized by a large aerosol loading associated with significant AOT. Over this specific region, the situation is dominated by

ACPD
11, 28587–28626, 2011

biomass burning aerosols during the dry season. In this work, simulated AOT reach maximum values (~0.65-0.80 at 500 nm) during DJF (between 0–10°N Latitude and centred around Longitude 20°E, see Fig. 1). The position of this "hot spot" of AOT is logically associated with the maximum emission of the bbAMMA inventories (Liousse et al., 2010) used in this study. Indeed, intense fires occur in the entire sahelian belt during the dry season (e.g. Roy et al., 2008) and the maximum of burnt vegetation surface observed by SPOT is located at the east of longitude 15°E (Chang and Song, 2009). Consequently, simulated AOT are significant in this part of the domain due to important burden of smoke aerosols. Comparisons with MODIS, OMI and MISR observations show lower AOT during the dry season with respectively AOT of 0.37, 0.43 and 0.35 (at ~500 nm) averaged over the central part of the continent (5° S–10° N, 13° E–30° E) compared to RegCM (0.49 at 500 nm). Moreover, the maximum of AOT observed by the different sensors is located slightly southward (the maximum is centred along the equator) compared to RegCM simulations. We note that similar observations (not shown here) of a local maximum of the fine mode AOT, linked to smoke aerosols, are also seen by POLDER (Polarization and Directionality of the Earth's Reflectances) on the A-Train PARASOL spacecraft (see example in Malavelle et al. (2011) for the 2006 dry season).

The discrepancies between the amplitude and location of simulated and observed AOT in the eastern part of the continent could be due to different sources of errors:

- the k_{ext} value of smoke aerosols in RegCM is higher than values reported in the literature. It is thus possible that in parallel to satellite underestimation, RegCM overestimates AOT for smoke aerosols.

- the maximum of fire intensity occurs between 03:00 PM and 05:00 PM (e.g. Giglio, 2007), while the passing time of AQUA and TERRA is quite sooner during the day. Thus, satellite observations provide instantaneous information on the integrated and transported biomass burning aerosol. While for RegCM outputs, they provide AOT information for regular emissions all the day long that could cumulate

ACPD
11, 28587–28626, 2011

wherever transport is inefficiently resolved over the domain . One should note also that averaged RegCM AOT is based on all the daily values including day and night. Therefore the maximum AOT values observed by the satellite are not collocated in time with simulated aerosols fields. As mentioned by Sayer et al. (2010) the sampling of satellite and models is very different and decisions about data selection and aggregation may cause regional differences in model AOT (of up to 0.1) on monthly and annual timescales. Moreover, we choose the simplest method (i.e. equal weight averaging of the daily satellite data) to aggregate daily satellite AOT into seasonal averages. Levy et al. (2009) showed that the different aggregation, weighting, and averaging-order choices could lead to very different regional and global average mean values (varying by 30 % or more). These differences are due to complications of orbital geometry, regions of persistent cloudiness, and other factors, that greatly impact the satellite sampling with season and location. All these inconstancies may contribute to some extend to the differences noted between modelled and observed AOT fields.

– another possible explanation could be that satellites retrievals perform less accuratly over these BB source regions due to high AOD values screening most of the surface, or due to some albedo effect of the surface at this period of the year (bare soils). However, the MISR sensor which allows no assumption on the surface properties displays the same AOT pattern as in MODIS observations. Similar observations have been obtained using the PARASOL sensor (not shown). In addition, it should be noted that Chen et al. (2008) and Kahn et al. (2010) indicate that in case of high MISR AOT (> 0.5, at mid visible wavelengths), the lack of surface informations could create ambiguity resulting in an underestimation of MISR AOT. Besides, it has also been showed by Ichoku et al. (2003), that MODIS may underestimate AOT retrieval over Southern Africa when aerosol loading is high due to inadequate assumed value of SSA. Chu et al. (2002) report also that the uncertainty in aerosol model has a greater impact at high AOT values than uncertainties in surface reflectance assumptions.

ACPD
11, 28587–28626, 2011

3.2.2 AOT observed over ocean

MODIS and MISR AOT also shows maximum values over the Gulf of Guinea (~0.5–0.7 at 500 nm) during DJF (Fig. 1). OMI AOT over ocean is also significant but lower than AOT retrieved by the two other sensors. Possible causes could be related to pixel cloud contamination (OMI resolution is rather low, i.e. $13 \times 24\,km^2$ at nadir for the UV1 channel) in this region of high clouds occurrence. A second possible source of disagreement could be related to the increased uncertainties on AOT over ocean due the near-UV method. The satellites under-sampling over the Gulf of Guinea due to the high cloud cover may not emphasize the attributes of the true aerosol fields.

Our results indicate that the simulated RegCM AOT during that period are underestimated (with a maximum around 0.45 at 500 nm) compared to MODIS and MISR sensors. Some causes of disagreement could be related to both inaccurate model transport of aerosols from eastern part of the domain, together with possible underestimation of both dust and BB aerosol loads coming from the northern part of the continent and the western part of the Sahel, respectively. Indeed, Malavelle et al. (2011) show that the model underestimates dust aerosols burden in the lower troposphere under approximately latitude 15°N during the dry season. Santese et al. (2010) also reported in RegCM simulations an underestimate of dust aerosol amounts at locations far from the sources, particularly in the lower troposphere.

Concerning biomass burning aerosols, bbAMMA inventories may fail some fire sources in the western Sahel. Indeed, Chang and Song (2009) reported that the L3JRC product (used to construct bbAMMA inventories) identify not as much burnt area than MODIS burnt area product for land covered with grass, shrub, or sparse vegetation cover which are typical vegetation of the Sahelian region. Lehsten et al. (2009) estimated that burnt areas were underestimated by approximately 48 % and 35 % for tree and shrub vegetation cover types in Africa, respectively. In addition, the L3JRC product may miss some small-sized burn scars, such as those in cultivated and managed areas. This underestimation is likely to have a signature in the bbAMMA emissions that

ACPD
11, 28587–28626, 2011

possibly explains some of the underestimated AOT not only over the Gulf of Guinea but also at Djougou and Ilorin.

During JJA season, the AOT over ocean is in agreement in the Atlantic outflow dominated by dust aerosols. Over the golf of Guinea, biomass burning season in southern Africa takes place. RegCM AOT over this area is strongly overestimated due to the inadequate biomass burning optical properties in the model that were computed specifically from AMMA measurements standing for West African biomass burnings.

3.2.3 SSA

In this section, we consider the retrieval of aerosol SSA from OMI, MODIS Deep Blue and MISR sensors in order to evaluate the RegCM simulated SSA. As mentioned previously, it is crucial to constrain accurately SSA because it represents one of the major source of uncertainty in the aerosol direct radiative forcing computations (McComiskey et al., 2008).

The Fig. 2 is similar as Fig. 1 but presents SSA and AESSA for RegCM and the three sensors previously mentioned. Note that all SSA values are reported at a wavelength in the range of 440-470 nm except OMI SSA reported at 500 nm. As mentioned by Kalashnikova and Kahn (2008), particle property sensitivity diminishes for midvisible AOT below about 0.15, and over bright surfaces in the MISR product. In that frame, the averaged SSA correspond to values flagged for AOT> 0.2 at 440 nm. In Fig. 3, we have also reported the averaged SSA over the subdomains "Sahel", "Sahara" and "Atlantic Outflow" represented on Fig. 2.

The first main result obtained from Fig. 2 is that the three sensors display very different estimates of SSA both in wintertime and summertime.

ACPD
11, 28587–28626, 2011

During DJF, OMI SSA shows a distinct aerosol feature confined to a latitudinal belt between 10°N and 15°N likely to correspond to the area of biomass burning, with SSA values as low as 0.88 (at 500 nm). The eastern part of the domain seems to have lower SSA values than the western part illustrating the possible mixing of dust and BB aerosols over western Sahel. Over the Gulf of Guinea, OMI SSA are about 0.954 (at 500 nm) while over Sahara, slightly more absorbing values are observed (~0.943 at 500 nm, Fig. 3). We can also observe in OMI product higher SSA values (more scattering) over the Gulf of Guinea where mixed dust and absorbing BB aerosols are expected to be found. To some extend the SSA values observed over the gulf of Guinea can be interpreted as a mixture dominated by fine dust aerosols that are more scattering (high SSA ~0.98–0.99 at 550 nm, Osborne et al., 2008) than the coarser dust aerosols (McConnell et al., 2008) less efficiently advected toward long distances (Maring et al., 2003).

In parallel, during DJF, MISR SSA show the highest value over the Sahara (~0.967 at 440 nm, Fig. 3) and the lowest one (~0.91 at 440 nm, Fig. 2) in the central Africa were most of the absorbing aerosols are expected. Over the entire Sahelian subdomain the average MISR SSA is 0.953 illustrating the mixing of dust aerosols and biomass burning aerosols. Over the gulf of guinea, the SSA values are intermediate (~0.94 at 440 nm). It is interesting to note that during JJA, SSA of biomass burning aerosols from the southern part of the continent are seen more absorbing (~0.890 at 440 nm, Fig. 3) than in DJF. This illustrates the mixing of BB aerosols with dust aerosols during winter-time. We note that MISR SSA values in JJA (dust dominated mixing) show surprising contrasts in the transition area between land and ocean, with lower values over ocean.

The MODIS Deep Blue SSA retrievals does not display a large variability over the West African region. The MODIS algorithm is based on a few set of theoretical aerosols models determined from clustering analysis of aerosols optical properties (Omar et al., 2005; Levy et al., 2007). Each model is assigned with a predefined SSA value. The best model that is retained for fitting measured to look up radiances assigns its value of SSA to the retrievals. For the dust aerosols, Deep Blue retrievals assumes two type

ACPD
11, 28587–28626, 2011

of dust aerosols, one with a whiter color and one with a redder color (Hsu et al., 2004, 2006). Therefore, because Deep Blue algorithm only retrieves SSA values for dust scene, one can expect that the SSA averaged over such timescale doesn't represent a lot of variability due to number of dust aerosol models considered. Highest value of SSA are 0.944 and 0.946 (at 470 nm) during DJF and JJA respectively over the Sahel (Fig. 3) and 0.932 and 0.939 (at 470 nm) over the Sahara.

It is also worth mentioning that OMI, Deep Blue and MISR SSA during summertime tend to increase over Sahara. This could be explained by the accumulation of fine dust in the West African atmospheric background during that season.

The RegCM simulated SSA represent much more absorbing aerosols than satellite estimates. Similarly, we observe in RegCM outputs a consistent north to south gradient of SSA over land during the dry season. The highest values are in the northern part (0.889 at 440 nm, Fig. 3) of the domain dominated by dust aerosols, and the lowest values of SSA eastern Sahel (i.e. Central Africa) where biomass burning emissions are maximum (~0.83 at 440 nm, Fig. 2). This gradient is also observed in both OMI and MISR.

We note from Fig. 3 that retrieved SSA for dust aerosols regions are encompassed between 0.932 and 0.967 (at 470 nm) during the dry season over the Sahara subdomain illustrating that at least the retrievals observed a mixing of relatively absorbing (coarse dust) and more scattering (fine dust) dust aerosols. RegCM simulated SSA is 0.889 (at 440 nm) in this Sahara subdomain. In central Africa (i.e. Biomass Burning sources) the simulated SSA is far more absorbing than what is observed in OMI and MISR products; it points out the fact that RegCM SSA could be too much absorbing for BB aerosols. Nevertheless, it has been constrained in order to obtain BB SSA consistent with DABEX observations of smoke aerosols (Johnson et al., 2008b). It could point out also too strong emission of BB aerosols in comparison to dust emission and transport that occur in the RegCM model.

ACPD
11, 28587–28626, 2011

3.3 The spectral dependence of AOT and AAOT optical properties

In this section, we investigate how the spectral dependencies of AOT and AAOT are simulated compared to satellite products. Indeed Biomass Burning aerosols and dust aerosols have different spectral absorptive properties due to different size and composition (see e.g. Derimian et al., 2008a; Bergstrom et al., 2007; Russell et al., 2010). In that frame, we discuss here the simulated angstrom exponent (Eq. 1) of AOT and AAOT compared to satellite retrievals in order to better discriminate the aerosols sources and mixing.

3.3.1 Spectral dependence of AOT

We present in Fig. 4 the DJF AEAOT from RegCM and the three satellite sensors.The DJF MISR AEAOT displayed in Fig. 4 clearly exhibits the lowest values in the Saharan desert pointing out the source of coarse dust aerosols. The Deep Blue MODIS AEAOT over the Saharan region is comparable to MISR estimates but highlights the Bodélé source. In addition, OMI AEAOT shows comparable values of AEAOT over the desert but does not display any regional contrast. Over the Sahelian band, the MISR and OMI sensors display greater values of AEAOT consistent with a higher contribution of fine particles to the aerosol mixing. We note also that MISR AEAOT show higher values in the eastern part of the Sahelian belt (∼1.1–1.2) than in the western part (∼0.7–0.9), probably due to higher emissions of biomass burning aerosols. Over the Gulf of Guinea, MISR AEAOT shows intermediate values (∼0.6–0.7) between AEAOT observed over the Sahara (∼0–0.5) and those observed over the Sahel. In parallel, OMI AEAOT values over the Gulf of Guinea (∼0.5–0.6) are similar to those observed over Sahara but should be taken with caution as OMI AOT is less accurate over ocean.

The RegCM AEAOT clearly shows the same inconsistency as the one mentioned when compared with AERONET/PHOTON ones. Indeed, the northern part of the domain is associated with negative value where dust aerosols dominate the mixing. Over the Sahel and Gulf of Guinea, RegCM AEAOT increases in agreement with the

ACPD
11, 28587–28626, 2011

contribution of biomass burning aerosols.

Figure 4 represents the averaged AEAOT over the three subdomains represented in Fig. 2. It is interesting to note that in JJA, when dust aerosols are the only major contributor to the total bulk aerosols in western Africa, the AEAOT values for the three satellite products over the Sahel show higher values than in DJF whereas AEAOT remains constant in the Atlantic outflow illustrating the surface influence on AOT retrievals.

3.3.2 Spectral variation of aerosol absorbing properties

The wavelength dependence of the absorption is a function of the size of the particle (as AEAOT) and chemical composition of aerosols. Absorpting properties can be used to identify aerosols sources, differentiate black carbon to dusts and reduce ambiguities in aerosol composition or mixtures resulting from AEAOT study only. It is shown that the exponent of absorption have a $1/\lambda$ dependence for spherical particles if the refractive indices are constant (Bohren and Huffman, 1983). Several studies (e.g. Bergstrom et al., 2007; Russell et al., 2010) have used these absorption angström exponent to retrieve useful informations on aerosol type.

In order to get additional informations to distinguish the aerosol mixture, we have computed the AEAAOT over the three subdomains (Fig. 2) for DJF and JJA seasons in Fig. 4 (right side).

The satellite observations show values of AEAAOT ranging from 3 and up to 5 over the Sahara, slightly higher than the value of 2.34 for dust aerosols estimated by Bergstrom et al. (2007) based on the PRIDE campaign but comparable to the AEAAOT estimated by Russell et al. (2010) over AERONET/PHOTON dusty sites. Over the Sahel, the AEAAOT for the three sensors, is reaching values encompassed between 2 and 3. During DJF, this should be consistent with the fact that biomass burning aerosols (with AEAAOT ~1.45–2) should contribute to the total aerosol absorption and tend to decrease the value of AEAAOT. However, we note that during JJA, the AEAAOT increases only in MISR estimates to reach similar values as over the Sahara and the Atlantic outflow dominated by dust aerosols.

ACPD
11, 28587–28626, 2011

Figure 5 shows the AEAOT versus AEAAOT for the averaged sub domains estimated by the three sensors. It seems that the Saharan averages (pure dust) show the lowest values of AEAOT combined with the highest values of AEAAOT whereas over the Sahel, and during the dry season (when Biomass Burning aerosols are present), the AEAOT increases while AEAAOT decreases.

We clearly see some differences between simulated AEAAOT and satellite estimates. The RegCM simulated AEAAOT is slightly lower than 1 (the theoretical value for pure Black Carbon) which exhibits strong weakness of the aerosols spectral properties in the RegCM model. In that sense, the current aerosol optical properties need to be better refined in order to assess their radiative forcing and climatic impact in future studies.

4 Summary and concluding remarks

The aim of this work is to evaluate aerosol optical properties simulated by the RegCM3 model for a long term (2000–2006) simulation over the West Africa region. Compared to the available literature, this modelling work includes smoke particles in the calculation. As absorbing properties of particles are clearly known to represent a critical parameter concerning the aerosol-climate interactions, we conducted comparisons with (1) classical local AERONET/PHOTON inversions but also with (2) new original satellite (MODIS, OMI, MISR) products providing informations on aerosol absorbing properties. Hence, in addition to the AOT, we used the Absorbing Aerosol Optical Thickness (AAOT) and Single Scattering Albedo (SSA) variables to evaluate the simulated absorbing properties in RegCM3. Comparisons of the simulated spectral dependence of optical properties (i.e., which is not always reported in the literature) with surface and satellite observations are also reported.

Concerning AOT, our results display a relatively good agreement with local observations but some differences are underlined with satellite estimations, especially over Central Africa and Gulf of Guinea during summer time. Errors on biomass burning

ACPD
11, 28587–28626, 2011

emissions, together with satellite retrievals could explain the difference obtained over Central Africa. Above the Gulf of Guinea, satellite estimations could indicate the presence of dust particles, which are not correctly estimated by the RegCM model.

We observed in RegCM outputs a consistent north to south gradient of SSA over land during the dry season. The highest values are obtained in the northern part (0.89 at 440 nm) of the domain dominated by dust aerosols, and the lowest values of SSA eastern Sahel (i.e. Central Africa) where biomass burning emission are maximum (~0.83 at 440 nm). Although the North-South SSA gradient is also observed in both OMI and MISR sensors, the RegCM simulated SSA display much more absorbing aerosols than satellite estimates. It should be noted that our study reveals also large differences in satellite (OMI, MISR, MODIS deep blue) SSA retrievals over the West African region. Such differences do not allow for definitively conclude about the ability of RegCM to reproduce regional realistic SSA over this region.

Finally, our work highlights that the spectral dependence of aerosol optical properties is constrated over the domain, so that sources of aerosols and their influence in the atmospheric mixing can be tracked through satellite observations. This approach enabled us to exhibit strong weakness of the aerosol spectral properties in RegCM. In that sense, the current aerosol optical properties need to be better refined in order become a powerful tool of comparison with latest original satellite retrievals.

Acknowledgements. On the basis of a French initiative, AMMA was built by an international scientific group and is currently funded by a large number of agencies, especially from France, UK, US, and Africa. It has been the beneficiary of a major financial contribution from the European Community's Sixth Framework Research Programme. AMMA has been endorsed by IGBP (IGAC, ILEAPS) and WCRP (GEWEX, CLIVAR). Detailed information on scientific coordination and funding is available on the AMMA International web site (http://www.amma-international.org/). The authors would like also to thank the respective PI's of AERONET/PHOTON sites for the data collection. MISR data were obtained from the NASA Langley Research Center Atmospheric Science Data Center. OMI data used in this effort were acquired as part of the activities of NASA's Science Mission Directorate, and are archived and distributed by the Goddard Earth Sciences (GES) Data and Information Services Center

ACPD
11, 28587–28626, 2011

(DISC). MODIS data were obtained from Goddard Space Flight Center (GSFC) thought Level 1 and Atmosphere Archive and Distribution System (LAADS).

The publication of this article is financed by CNRS-INSU.

References

Ahn, C., Torres, O., and Bhartia, P. K.: Comparison of Ozone Monitoring Instrument UV Aerosol Products with Aqua/Moderate Resolution Imaging Spectroradiometer and Multi-angle Imaging Spectroradiometer observations in 2006, J. Geophys. Res., 113, D16S27, doi:10.1029/2007JD008832, 2008.

Alfaro, S. C. and Gomes, L.: Modelling mineral aerosol production by wind erosion: Emission intensities and aerosol size distributions in source areas, Geophys. Res. Lett., 106, 991–994, 2001.

Bergstrom, R. W., Pilewskie, P., Russell, P. B., Redemann, J., Bond, T. C., Quinn, P. K., and Sierau, B.: Spectral absorption properties of atmospheric aerosols, Atmos. Chem. Phys., 7, 5937–5943, doi:10.5194/acp-7-5937-2007, 2007.

Bohren, C. F. and Huffman, D. R.: Absorption and Scattering of Light by Small Particles, John Wiley, Hoboken, 82–129, 1983.

Cavazos, C., Todd, M. C., and Schepanski, K.: Numerical model simulation of the Saharan dust event of 6-11 March 2006 using the Regional Climate Model version 3 (RegCM3), J. Geophys. Res., 114, D12109, doi:10.1029/2008JD011078, 2009.

Chang, D. and Song, Y.: Comparison of L3JRC and MODIS global burned area products from 2000 to 2007, J. Geophys. Res., 114, D16106, doi:10.1029/2008JD011361, 2009.

Chen, T.-C., Wang, S.-Y., and Clark, A. J.: North Atlantic hurricanes contributed by African easterly waves North and South of the African easterly jet, J. Climate, 21, 6767–6776, 2008.

ACPD
11, 28587–28626, 2011

Chu, D. A., Kaufman, Y. J., Ichoku, C., Remer, L. A., Tanré, D., and Holben, B. N.: Validation of MODIS aerosol optical depth retrieval over land, Geophys. Res. Lett., 29, 8007, doi:10.1029/2001GL013205, 2002.

Cooke, W. F., Liousse, C., Cachier, H., and Feichter, J.: Construction of a 1°×1° fossil fuel emission data set for carbonaceous aerosol and implementation and radiative impact in the ECHAM4 model, J. Geophys. Res., 104, 162, D18, doi:10.1029/1999JD900187, 1999.

Crumeyrolle, S., Tulet, P., Gomes, L., Garcia-Carreras, L., Flamant, C., Parker, D. J., Matsuki, A., Formenti, P., and Schwarzenboeck, A.: Transport of dust particles from the Bodélé region to the monsoon layer – AMMA case study of the 9–14 June 2006 period, Atmos. Chem. Phys., 11, 479–494, doi:10.5194/acp-11-479-2011, 2011.

Dall'Osto, M., Ceburnis, D., Martucci, G., Bialek, J., Dupuy, R., Jennings, S. G., Berresheim, H., Wenger, J., Healy, R., Facchini, M. C., Rinaldi, M., Giulianelli, L., Finessi, E., Worsnop, D., Ehn, M., Mikkilä, J., Kulmala, M., and O'Dowd, C. D.: Aerosol properties associated with air masses arriving into the North East Atlantic during the 2008 Mace Head EUCAARI intensive observing period: an overview, Atmos. Chem. Phys., 10, 8413–8435, doi:10.5194/acp-10-8413-2010, 2010.

Derimian, Y., Karnieli, A., Kaufman, Y. J., Andreae, M. O., Andreae, T. W., Dubovik, O., Maenhaut, W., and Koren, I.: The role of iron and black carbon in aerosol light absorption, Atmos. Chem. Phys., 8, 3623–3637, doi:10.5194/acp-8-3623-2008, 2008.

Diner, D., Beckert, J., Reilly, T., Bruegge, C., Conel, J., Kahn, R., Martonchik, J., Ackerman, T., Davies, R., Gerstl, S., Gordon, H., Muller, J.-P., Myneni, R., Sellers, P., Pinty, B., and Verstraete, M.: Multi-angle Imaging SpectroRadiometer (MISR) instrument description and experiment overview, IEEE T. Geosci. Remote, 36, 1072–1087, 1998.

Dubovik, O., Smirnov, A., Holben, B. N., King, M. D., Kaufmann, Y. J., Eck, T. F., and Slutsker, I.: Accuracy assessments of aerosol properties retrieved from Aerosol Robotic Network (AERONET) sun and sky radiance measurements, J. Geophys. Res., 105, 9791–9806, 2000.

Dubovik, O., Holben, B., Eck, T. F., Smirnov, A., Kaufman, Y. J., King, M. D., Tanré, D., and Slutsker, I.: Variability of Absorption and Optical Properties of Key Aerosol Types Observed in Worldwide Locations, 59, 590–608, 2002.

Dubovik, O., Herman, M., Holdak, A., Lapyonok, T., Tanré, D., Deuzé, J. L., Ducos, F., Sinyuk, A., and Lopatin, A.: Statistically optimized inversion algorithm for enhanced retrieval of aerosol properties from spectral multi-angle polarimetric satellite observations, Atmos. Meas.

ACPD

11, 28587–28626, 2011

Tech., 4, 975–1018, doi:10.5194/amt-4-975-2011, 2011.
Giglio, L.: Characterization of the tropical diurnal fire cycle using VIRS and MODIS observations, Remote Sens. Environ., 108, 407–421, 2007.
Giorgi, F. and Mearns, L. O.: Introduction to special section: Regional climate modeling revisited, J. Geophys. Res., 104, 6335–6352, 1999.
Grini, A., Tulet, P., and Gomes, L.: Dusty weather forecast using the mesonh atmospheric model, J. Geophys. Res., 111, D19205, doi:10.1029/2005JD007007, 2006.
Haywood, J. M., Osborne, S. R., Francis, P. N., Keil, A., Formenti, P., Andreae, M. O., and Kaye, P. H.: The mean physical and optical properties of regional haze dominated by biomass burning aerosol measured from the C-130 aircraft during SAFARI 2000, J. Geophys. Res., 108, 8473, doi:10.1029/2002JD002226, 2003.
Haywood, J. M., Pelon, J., Formenti, P., Bharmal, N., Brooks, M., Capes, G., Chazette, P., Chou, C., Christopher, S., Coe, H., Cuesta, J., Derimian, Y., Desboeufs, K., Greed, G., Harrison, M., Heese, B., Highwood, E. J., Johnson, B., Mallet, M., Marticorena, B., Marsham, J., Milton, S., Myhre, G., Osborne, S. R., Parker, D. J., Rajot, J.-L., Schultz, M., Slingo, A., Tanré, D., and Tulet, P.: Overview of the Dust and Biomass-burning Experiment and African Monsoon Multidisciplinary Analysis Special Observing Period-0, J. Geophys. Res., 113, D00C17, doi:10.1029/2008JD010077, 2008.
Heinold, B., Helmert, J., Hellmuth, O., Wolke, R., Ansmann, A., Marticorena, B., Laurent, B., and Tegen, I.: Regional modeling of Saharan dust events using LM-MUSCAT: Model description and case studies, J. Geophys. Res., 112, D11204, doi:10.1029/2006JD007443, 2007.
Holben, B., Eck, T., Slutsker, I., Tanré, D., Buis, J., and Setzer, A.: AERONET - A federated instrument network and data archive for aerosol characterization, Remote Sens. Environ., 66, 1–16, 1998.
Hsu, N., Tsay, S., King, M., and Herman, J.: Aerosol properties over bright-reflecting source regions, IEEE T. Geosci. Remote, 42, 557–569, 2004.
Hsu, N., Tsay, S., King, M., and Herman, J.: Deep Blue Retrievals of Asian Aerosol Properties During ACE-Asia, IEEE T. Geosci. Remote, 44, 3180–3195, 2006.
Huang, J., Zhang, C., and Prospero, J. M.: Large-scale effect of aerosols on precipitation in the West African monsoon region, Q. J. Roy. Meteorol. Soc., 135, 581–594, 2009a.
Huang, J., Zhang, C., and Prospero, J. M.: African aerosol and large-scale precipitation variability over West Africa, Environ. Res. Lett., 4, 015 006, doi:10.1088/1748-9326/4/1/015006,

ACPD
11, 28587–28626, 2011

2009b.
Ichoku, C., Remer, L. A., Kaufman, Y. J., Levy, R., Chu, D. A., Tanré, D., and Holben, B. N.: MODIS observation of aerosols and estimation of aerosol radiative forcing over southern Africa during SAFARI 2000, J. Geophys. Res., 108, 13pp., 2003.
Jethva, H. and Torres, O.: Satellite-based evidence of wavelength-dependent aerosol absorption in biomass burning smoke inferred from ozone monitoring instrument, Atmos. Chem. Phys. Discuss., 11, 7291–7319, doi:10.5194/acpd-11-7291-2011, 2011.
Johnson, B., Osborne, S., Haywood, J., and Harrison, M.: Aircraft measurements of biomass burning aerosol over West Africa during DABEX, J. Geophys. Res., 113, D00C06, doi:10.1029/2007JD009451, 2008.
Junker, C. and Liousse, C.: A global emission inventory of carbonaceous aerosol from historic records of fossil fuel and biofuel consumption for the period 1860–1997, Atmos. Chem. Phys., 8, 1195–1207, doi:10.5194/acp-8-1195-2008, 2008.
Kahn, R. A., Gaitley, B. J., Garay, M. J., Diner, D. J., Eck, T. F., Smirnov, A., and Holben, B. N.: Multiangle Imaging SpectroRadiometer global aerosol product assessment by comparison with the Aerosol Robotic Network, J. Geophys. Res., 115, D23209, doi:10.1029/2010JD014601, 2010.
Kalashnikova, O. V. and Kahn, R. A.: Mineral dust plume evolution over the Atlantic from MISR and MODIS aerosol retrievals, J. Geophys. Res., 113, D12206, D24204, doi:10.1029/2008JD010083, 2008.
Kaufman, Y. J., Tanré, D., Remer, L. A., Vermote, E. F., Chu, A., and Holben, B. N.: Operational remote sensing of tropospheric aerosol over land from EOS moderate resolution imaging spectroradiometer, J. Geophys. Res., 102, 17051–17067, 1997.
Klüser, L. and Holzer-Popp, T.: Relationships between mineral dust and cloud properties in the West African Sahel, Atmos. Chem. Phys., 10, 6901–6915, doi:10.5194/acp-10-6901-2010, 2010.
Konare, A., Zakey, A. S., Solmon, F., Giorgi, F., Rauscher, S., Ibrah, S., and Bi, X.: A regional climate modeling study of the effect of desert dust on the West African monsoon, J. Geophys. Res., 113, D12206, doi:10.1029/2007JD009322, 2008.
Lau, K. M., Kim, K. M., Sud, Y. C., and Walker, G. K.: A GCM study of the response of the atmospheric water cycle of West Africa and the Atlantic to Saharan dust radiative forcing, Ann. Geophys., 27, 4023–4037, doi:10.5194/angeo-27-4023-2009, 2009.
Lehsten, V., Tansey, K., Balzter, H., Thonicke, K., Spessa, A., Weber, U., Smith, B., and

ACPD
11, 28587–28626, 2011

Arneth, A.: Estimating carbon emissions from African wildfires, Biogeosciences, 6, 349–360, doi:10.5194/bg-6-349-2009, 2009.
Levelt, P., van den Oord, G., Dobber, M., Malkki, A., Visser, H., de Vries, J., Stammes, P., Lundell, J., and Saari, H.: The Ozone Monitoring Instrument, IEEE T. Geosci. Remote, 44, 1093–1101, 2006.
Levy, R., Leptoukh, G., Kahn, R., Zubko, V., Gopalan, A., and Remer, L.: A Critical Look at Deriving Monthly Aerosol Optical Depth From Satellite Data, IEEE T. Geosci. Remote, 47, 2942–2956, 2009.
Levy, R. C., Remer, L. A., and Dubovik, O.: Global aerosol optical properties and application to Moderate Resolution Imaging Spectroradiometer aerosol retrieval over land, J. Geophys. Res., 112, D13210, doi:10.1029/2006JD007815, 2007.
Liousse, C., Penner, J. E., Chuang, C., Walton, J. J., Eddleman, H., and Cachier, H.: A global threedimensional model study of carbonaceous aerosols, J. Geophys. Res., 101, 19,411–19, doi:10.1029/95JD03426, 1996.
Liousse, C., Andreae, M. O., Artaxo, P., Barbosa, P., Cachier, H., Grégoire, J., Hobbs, P., Lavoué, D., Mouillot, F., Penner, J., Scholes, M., and Schultz, M. G.: Deriving global quantitative estimates for spatial and temporal distributions of biomass burning emissions, in: Emissions of atmospheric trace compounds, edited by Granier, C., Artaxo, P., and Reeves, C. E., chap. 3, Kluwer Academic Publ., 77–120, 2004.
Liousse, C., Guillaume, B., Grégoire, J. M., Mallet, M., Galy, C., Pont, V., Akpo, A., Bedou, M., Castéra, P., Dungall, L., Gardrat, E., Granier, C., Konaré, A., Malavelle, F., Mariscal, A., Mieville, A., Rosset, R., Serça, D., Solmon, F., Tummon, F., Assamoi, E., Yoboué, V., and Velthoven, P. V.: Updated African biomass burning emission inventories in the framework of the AMMA-IDAF program, with an evaluation of combustion aerosols, Atmos. Chem. Phys., 10, 9631–9646, doi:10.5194/acp-10-9631-2010, 2010.
Malavelle, F., Pont, V., Mallet, M., Solmon, F., Johnson, B., Leon, J., and Liousse, C.: Simulation of aerosol radiative effects over West Africa during DABEX and AMMA SOP-0, J. Geophys. Res., 116, 2011.
Mallet, M., Pont, V., Liousse, C., Gomes, L., Pelon, J., Osborne, S., Haywood, J., Roger, J., Dubuisson, P., Mariscal, A., Thouret, V., and Goloub, P.: Aerosol direct radiative forcing over Djougou (northern Benin) during the African Monsoon Multidisciplinary Analysis dry season experiment (Special Observation Period-0), J. Geophys. Res., 113, D00C01, doi:10.1029/2007JD009419, 2008.

ACPD
11, 28587–28626, 2011

Mallet, M., Tulet, P., Serça, D., Solmon, F., Dubovik, O., Pelon, J., Pont, V., and Thouron, O.: Impact of dust aerosols on the radiative budget, surface heat fluxes, heating rate profiles and convective activity over West Africa during March 2006, Atmos. Chem. Phys., 9, 7143–7160, doi:10.5194/acp-9-7143-2009, 2009.

Maring, H., Savoie, D. L., Izaguirre, M. A., Custals, L., and Reid, J. S.: Mineral dust aerosol size distribution change during atmospheric transport, J. Geophys. Res., 108, 1–6, doi:10.1029/2002JD002536, 2003.

Marticorena, B. and Bergametti, G.: Modeling the atmospheric dust cycle: 1-Designed of a soilderived dust emissions, J. Geophys. Res., 100, 16415–16430, 1995.

McComiskey, A., Schwartz, S. E., Schmid, B., Guan, H., Lewis, E. R., Ricchiazzi, P., and Ogren, J. A.: Direct aerosol forcing: Calculation from observables and sensitivities to inputs, J. Geophys. Res., 113, D09202, doi:10.1029/2007JD009170, 2008.

McConnell, C. L., Highwood, E. J., Coe, H., Formenti, P., Anderson, B., Osborne, S., Nava, S., Desboeufs, K., Chen, G., and Harrison, M. A. J.: Seasonal variations of the physical and optical characteristics of Saharan dust: Results from the Dust Outflow and Deposition to the Ocean (DODO) experiment, J. Geophys. Res., 113, 19 pp., 2008.

McConnell, C. L., Formenti, P., Highwood, E. J., and Harrison, M. A. J.: Using aircraft measurements to determine the refractive index of Saharan dust during the DODO Experiments, Atmos. Chem. Phys., 10, 3081–3098, doi:10.5194/acp-10-3081-2010, 2010.

Michel, C., Liousse, C., Grégoire, J., Tansey, K., Carmichael, G. R., and Woo, J.: Biomass burning emission inventory from burnt area data given by the SPOT-VEGETATION system in the frame of TRACE-P and ACE-Asia campaigns, J. Geophys. Res., 110, 15 pp., 2005.

Milton, S. F., Greed, G., Brooks, M. E., Haywood, J., Johnson, B., Allan, R. P., Slingo, A., and Grey, W. M. F.: Modeled and observed atmospheric radiation balance during the West African dry season: Role of mineral dust, biomass burning aerosol, and surface albedo, J. Geophys. Res., 113, D00C02, doi:10.1029/2007JD009741, 2008.

Myhre, G., Grini, A., Haywood, J. M., Stordal, F., Chatenet, B., Tanré, D., Sundet, J. K., and Isaksen, I. S. A.: Modeling the radiative impact of mineral dust during the Saharan Dust Experiment (SHADE) campaign, J. Geophys. Res., 108, 8579, doi:10.1029/2002JD002566, 2003.

Myhre, G., Hoyle, C. R., Berglen, T. F., Johnson, B. T., and Haywood, J. M.: Modeling of the solar radiative impact of biomass burning aerosols during the Dust and Biomass-burning Experiment (DABEX), J. Geophys. Res., 113, D00C16, doi:10.1029/2008JD009857, 2008.

ACPD
11, 28587–28626, 2011

Omar, A. H., Won, J., Winker, D. M., Yoon, S., Dubovik, O., and McCormick, M. P.: Development of global aerosol models using cluster analysis of Aerosol Robotic Network (AERONET) measurements, J. Geophys. Res., 110, D10S14, doi:10.1029/2004JD004874, 2005.
Osborne, S. R., Johnson, B. T., Haywood, J. M., Baran, A. J., Harrison, M. A. J., and McConnell, C. L.: Physical and optical properties of mineral dust aerosol during the Dust and Biomass-burning Experiment, J. Geophys. Res., 113, D00C03, doi:10.1029/2007JD009551, 2008.
Pal, J. S., Giorgi, F., Bi, X., Elguindi, N., Solmon, F., Gao, X., Rauscher, S. A., Franscico, R., Zakey, A., Winter, J., Ashfaq, M., Syed, F. S., Bell, J. L., Diffenbauch, N. S., Karmacharya, J., Konare, A., Martinez, D., Da Rocha, R. P., Sloan, L. C., and Steiner, A. L.: Regional climate modeling for the developing world: the ICTP RegCM3 and RegCNET, B. Am. Meteorol. Soc., 88, 1395–1409, 2007.
Perlwitz, J. and Miller, R. L.: Cloud cover increase with increasing aerosol absorptivity: A counterexample to the conventional semidirect aerosol effect, J. Geophys. Res., 115, D08203, doi:10.1029/2009JD012637, 2010.
Pont, V., Mallet, M., Liousse, C., Gomes, L., Malavelle, F., Solmon, F., Galy, C., Gardrat, E., and Castéra, P.: Mixing of dust and carbonaceous aerosols: three concepts of chemical scheme from AMMA dry season experiment (SOP0 – January 2006) at Djougou (Benin), in: AMMA Conference, Ouagadougou (Burkina Faso), 2009.
Prospero, J. and Lamb, P.: African droughts and dust transport to the Caribbean: Climate change implication, Science, 302, 1024–1027, doi:10.1126/science.1089915, 2003.
Reid, J. S., Eck, T. F., Christopher, S. A., Koppmann, R., Dubovik, O., Eleuterio, D. P., Holben, B. N., Reid, E. A., and Zhang, J.: A review of biomass burning emissions part III: intensive optical properties of biomass burning particles, Atmos. Chem. Phys., 5, 827–849, doi:10.5194/acp-5-827-2005, 2005.
Remer, L. A., Kaufman, Y. J., Tanré, D., Mattoo, S., Chu, D. A., Martins, J. V., Li, R., Ichoku, C., Levy, R. C., Kleidman, R. G., Eck, T. F., Vermote, E., and Holben, B. N.: The MODIS Aerosol Algorithm, Products, and Validation, J. Atmos. Sci., 62, 947, 2005.
Roy, D., Boschetti, L., Justice, C., and Ju, J.: The collection 5 MODIS burned area product – Global evaluation by comparison with the MODIS active fire product, Remote Sens. Environ., 112, 3690–3707, 2008.
Russell, P. B., Bergstrom, R. W., Shinozuka, Y., Clarke, A. D., DeCarlo, P. F., Jimenez, J. L., Livingston, J. M., Redemann, J., Dubovik, O., and Strawa, A.: Absorption Angstrom Exponent in AERONET and related data as an indicator of aerosol composition, Atmos.

ACPD
11, 28587–28626, 2011

Chem. Phys., 10, 1155–1169, doi:10.5194/acp-10-1155-2010, 2010.
Santese, M., Perrone, M. R., Zakey, A. S., De Tomasi, F., and Giorgi, F.: Modeling of Saharan dust outbreaks over the Mediterranean by RegCM3: case studies, Atmos. Chem. Phys., 10, 133–156, doi:10.5194/acp-10-133-2010, 2010.
Sayer, A. M., Thomas, G. E., Palmer, P. I., and Grainger, R. G.: Some implications of sampling choices on comparisons between satellite and model aerosol optical depth fields, Atmos. Chem. Phys., 10, 10705–10716, doi:10.5194/acp-10-10705-2010, 2010.
Schepanski, K., Tegen, I., and Macke, A.: Saharan dust transport and deposition towards the tropical northern Atlantic, Atmos. Chem. Phys., 9, 1173–1189, doi:10.5194/acp-9-1173-2009, 2009.
Simmons, A., Uppala, S., Dee, D., and Kobayashi, S.: ERA-Interim: New ECMWF reanalysis products from 1989 onwards, ECMWF Newsletter, 110, 25–35, 2007.
Slingo, A., Ackerman, T. P., Allan, R. P., Kassianov, E. I., McFarlane, S. A., Robinson, G. J., Barnard, J. C., Miller, M. A., Harries, J. E., Russell, J. E., and Dewitte, S.: Observations of the impact of a major Saharan dust storm on the atmospheric radiation balance, Geophys. Res. Lett., 33, L24817, doi:10.1029/2006GL027869, 2006.
Slingo, A., White, H. E., Bharmal, N. A., and Robinson, G. J.: Overview of observations from the RADAGAST experiment in Niamey, Niger: 2. Radiative fluxes and divergences, J. Geophys. Res., 114, D00E04, doi:10.1029/2008JD010497, 2009.
Solmon, F., Mallet, M., Elguindi, N., Giorgi, F., Zakey, A., and Konaré, A.: Dust aerosol impact on regional precipitation over western Africa, mechanisms and sensitivity to absorption properties, Geophys. Res. Lett., 35, L24705, doi:10.1029/2008GL035900, 2008.
Sud, Y. C., Wilcox, E., Lau, W. K.-M., Walker, G. K., Liu, X.-H., Nenes, A., Lee, D., Kim, K.-M., Zhou, Y., and Bhattacharjee, P. S.: Sensitivity of boreal-summer circulation and precipitation to atmospheric aerosols in selected regions – Part 1: Africa and India, Ann. Geophys., 27, 3989–4007, doi:10.5194/angeo-27-3989-2009, 2009.
Tanré, D., Kaufman, Y. J., Herman, M., and Mattoo, S.: Remote sensing of aerosol properties over oceans using the MODIS/EOS spectral radiances, J. Geophys. Res., 102, 16971–16988, 1997.
Tanré, D., Bréon, F. M., Deuzé, J. L., Herman, M., Goloub, P., Nadal, F., and Marchand, A.: Global observation of anthropogenic aerosols from satellite, Geophys. Res. Lett., 28, 4555–4558, 2001.
Todd, M. C., Karam, D. B., Cavazos, C., Bouet, C., Heinold, B., Baldasano, J. M., Cautenet,

ACPD
11, 28587–28626, 2011

G., Koren, I., Perez, C., Solmon, F., Tegen, I., Tulet, P., Washington, R., and Zakey, A.: Quantifying uncertainty in estimates of mineral dust flux: An intercomparison of model performance over the Bodélé Depression, northern Chad, J. Geophys. Res., 113, D24107, doi:10.1029/2008JD010476, 2008.

Torres, O., Bhartia, P. K., Herman, J. R., Ahmad, Z., and Gleason, J.: Derivation of aerosol properties from satellite measurements of backscattered ultraviolet radiation: Theoretical basis, J. Geophys. Res., 103, 17099–17110, 1998.

Torres, O., Tanskanen, A., Veihelmann, B., Ahn, C., Braak, R., Bhartia, P. K., Veefkind, P., and Levelt, P.: Aerosols and surface UV products from Ozone Monitoring Instrument observations: An overview, J. Geophys. Res., 112, D24S47, doi:10.1029/2007JD008809, 2007.

Tulet, P., Mallet, M., Pont, V., Pelon, J., and Boone, A.: The 7–13 Marh 2006 dust storm over West Africa: generation, transport and vertical stratification, J. Geophys. Res., 113, D00C08, doi:10.1029/2008JD009871, 2008.

van derWerf,G. R., Randerson, J. T., Giglio, L., Collatz,G. J., Kasibhatla, P. S., and Jr., A. F. A.: Interannual variability in global biomass burning emissions from 1997 to 2004, Atmos. Chem. Phys., 6, 3423–3441, vdoi:10.5194/acp-6-3423-2006, 2006.

Yoshioka, M., Mahowald, N. M., Conley, A. J., Collins, W. D., Fillmore, D. W., Zender, C. S., and Coleman, D. B.: Impact of desert dust radiative forcing on Sahel precipitation: relative importance of dust compare to sea surface temperature variations, vegetation changes and greenhouse gas warming, J. Climate, 20, 1445–1467, doi:10.1175/JCLI4056.1, 2007.

Zakey, A. S., Solmon, F., and Giorgi, F.: Implementation and testing of a desert dust module in a regional climate model, Atmos. Chem. Phys., 6, 4687–4704, doi:10.5194/acp-6-4687-2006, 2006.

Zhao, C., Liu, X., Leung, L. R., and Hagos, S.: Radiative impact of mineral dust on monsoon precipitation variability over West Africa, Atmos. Chem. Phys., 11, 1879–1893, doi:10.5194/acp-11-1879-2011, 2011.

ACPD
11, 28587–28626, 2011

Table 1. Mean dry optical properties for BC and OC and DUST tracers used in the RegCM simulations presented here.

	BC			OC								
Wavelength (nm)	440	500	675	440	500	675						
Kext ($m^2\ g^{-1}$)	16.90	14.12	12.03	6.46	5.06	4.06						
SSA	0.394	0.386	0.395	0.921	0.918	0.914						
g	0.618	0.590	0.560	0.690	0.650	0.668						
	DUST Bin 1			DUST Bin 2			DUST Bin 3			DUST Bin 4		
Wavelength (nm)	440	500	675	440	500	675	440	500	675	440	500	675
Kext ($g^2\ m^{-1}$)	1.89	2.45	2.93	0.777	0.86	0.75	0.36	0.38	0.44	0.18	0.17	0.19
SSA	0.935	0.958	0.974	0.873	0.904	0.876	0.777	0.825	0.862	0.693	0.709	0.764
g	0.609	0.644	0.746	0.778	0.765	0.549	0.801	0.813	0.807	0.888	0.878	0.860

ACPD
11, 28587–28626, 2011

Table 2. Comparison of averaged DJF and JJA AOT, SSA and AOT Angstrom Exponent (AE) from RegCM, AERONET/PHOTON, MISR and Modis (Deep Blue) for the site of Agoufou, Ilorin, Banizoumbou, Capo Verde and Djougou for data available between January 2001 and December 2006.

		AGOUFOU (15° N,1° W)		ILORIN (8° N,4° E)		BANIZOUMBOU (13° N,2° E)		CAPO VERDE (16° N,22° W)		DJOUGOU (9° N,1° E)	
		DJF	JJA	DJF	JJA	DJF	JJA	DJF	JJA	DJF	JJA
RegCM3	$\tau_{440/675}$	0.36/0.46	0.50/0.70	0.41/0.41	0.21/0.28	0.32/0.40	0.35/0.50	0.22/0.30	0.47/0.68	0.37/0.38	0.24/0.33
	$SSA_{440/675}$	0.873/0.926	0.892/0.943	0.838/0.885	0.882/0.935	0.879/0.930	0.905/0.953	0.902/0.950	0.913/0.958	0.850/0.900	0.899/0.948
	$AE_{440/675}$	−0.53	−0.78	−0.05	−0.59	−0.49	−0.82	−0.70	−0.87	−0.14	−0.71
AERONET	$\tau_{440/675}$	0.43/0.38	0.65/0.63	1.00/0.76	0.43/0.31	0.47/0.41	0.51/0.46	0.26/0.22	0.50/0.46	0.84/0.66	0.69/0.60
	$SSA_{440/675}$	0.890/0.936	0.891/0.943	0.871/0.904	0.913/0.920	0.919/0.961	0.922/0.955	0.858/0.897	0.913/0.962	0.838/0.872	0.913/0.917
	[1]$AE_{440/870}$	0.41	0.14	0.72	0.84	0.21	0.42	0.44	0.19	0.74	0.69
MISR	$\tau_{443/675}$	0.34/0.28	0.65/0.52	0.64/0.47	0.36/0.20	0.40/0.33	0.59/0.45	0.30/0.24	0.62/0.53	0.53/0.41	0.29/0.18
	$SSA_{443/675}$	0.967/0.988	0.961/0.993	0.955/0.977	0.956/0.968	0.972/0.993	0.968/0.993	0.945/0.986	0.940/0.991	0.958/0.980	0.950/0.954
	[2]AE	0.56	0.54	0.69	1.43	0.53	0.68	0.54	0.36	0.65	1.16
MODIS (Deep Blue)	$\tau_{440/660}$	0.52/0.38	0.67/0.62	NA/NA	NA/NA	0.59/0.41	0.71/0.57	0.20/0.13	0.54/0.60	0.66/0.40	0.30/0.21
	$SSA_{440/660}$	0.933/0.974	0.923/0.974	NA/NA	NA/NA	0.935/0.974	0.923/0.974	0.937/0.975	0.925/0.975	0.953/0.975	0.934/0.975
	[3]$AE_{412/470}$	0.75	0.30	NA/NA	NA/NA	0.89	0.59	0.99	−0.18	1.10	0.93

[1] For AERONET data we have reported the AE from the skyradiance measurements

[2] MISR AE is estimated from the four channels (443, 555, 670, 875 nm) measurements

[3] Deep Blue AE is provided between 412 and 470 nm. The range of Deep Blue AE is −0.5 to 5.

ACPD
11, 28587–28626, 2011

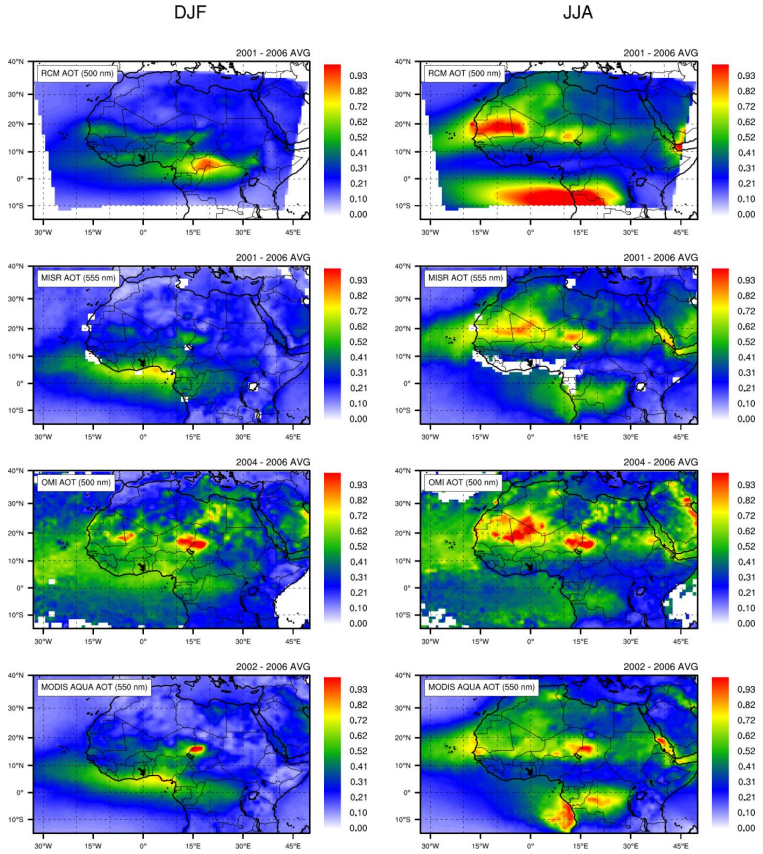

Fig. 1. Aerosols optical thickness averaged between 2001 and 2006. First row, RegCM (at 500 nm), Second Row MISR (at 555nm), third Row MODIS/DEEP BLUE (at 550 nm between 2002 and 2006), last row OMI (at 500 nm between 2004 and 2006). Left Side panel: DJF Average, Right side panel: JJA average. All presented data have been re-aggregated on a $1^{\circ} \times 1^{\circ}$ regular grid.

ACPD
11, 28587–28626, 2011

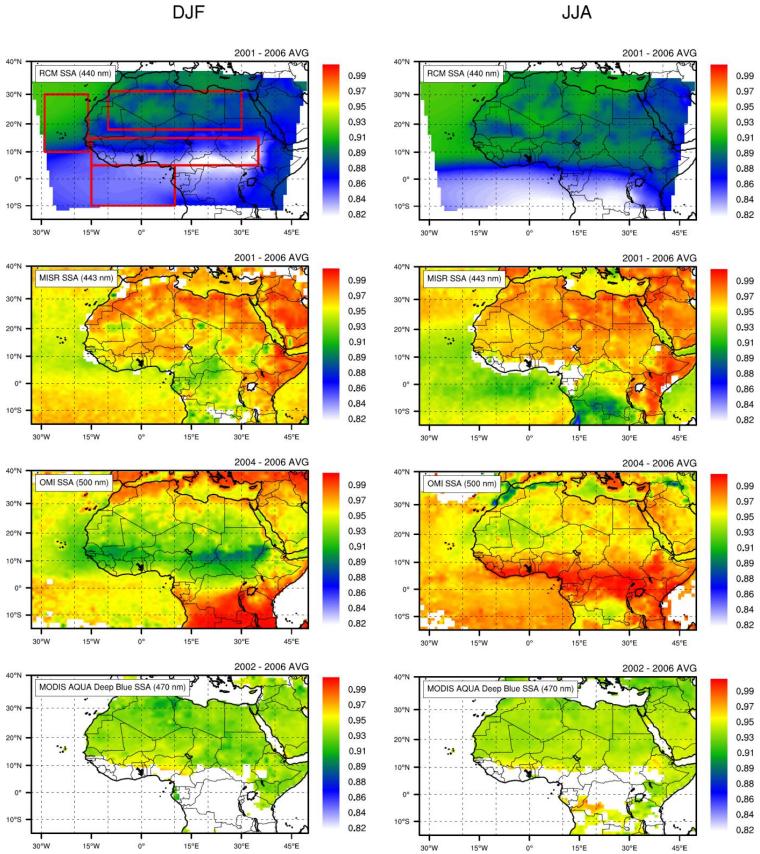

Fig. 2. Similar as Fig. 1 but for aerosol Single Scattering Albedo at 440nm (500 nm for OMI SSA).

ACPD
11, 28587–28626, 2011

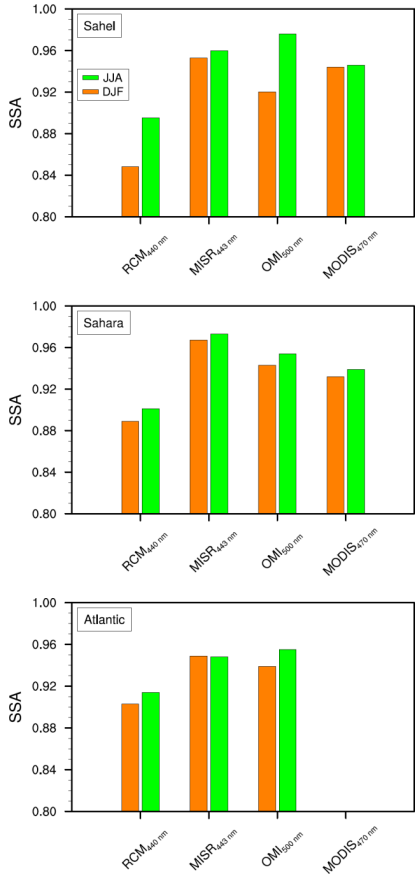

Fig. 3. Averaged SSA at 440 nm (500 nm for OMI) over the subdomains represented in Fig. 2 for DJF and JJA.

ACPD
11, 28587–28626, 2011

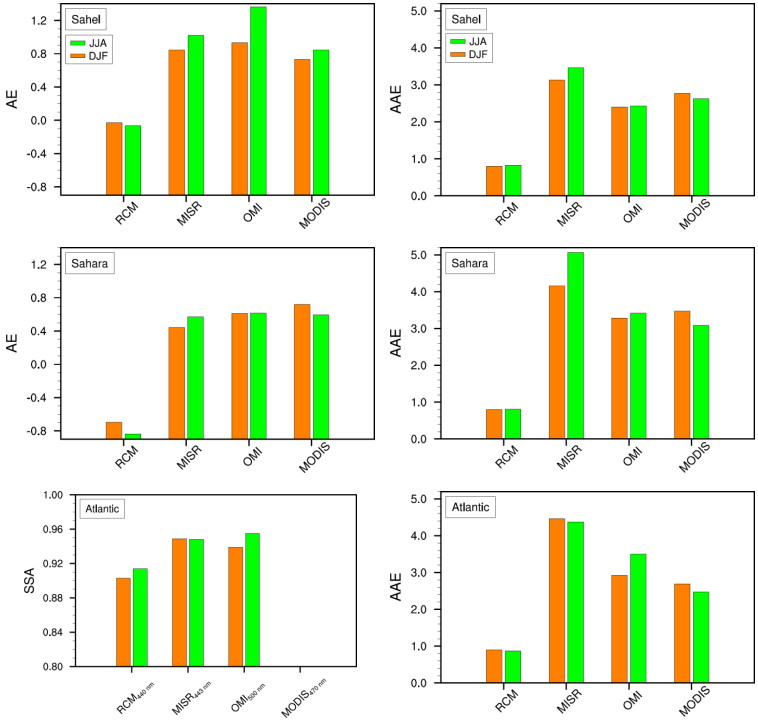

Fig. 4. Averaged AOT Angstrom exponent (left side) and AOT Absorption Angstrom exponent (right side) over the subdomains represented in Fig. 2 for DJF and JJA.

ACPD
11, 28587–28626, 2011

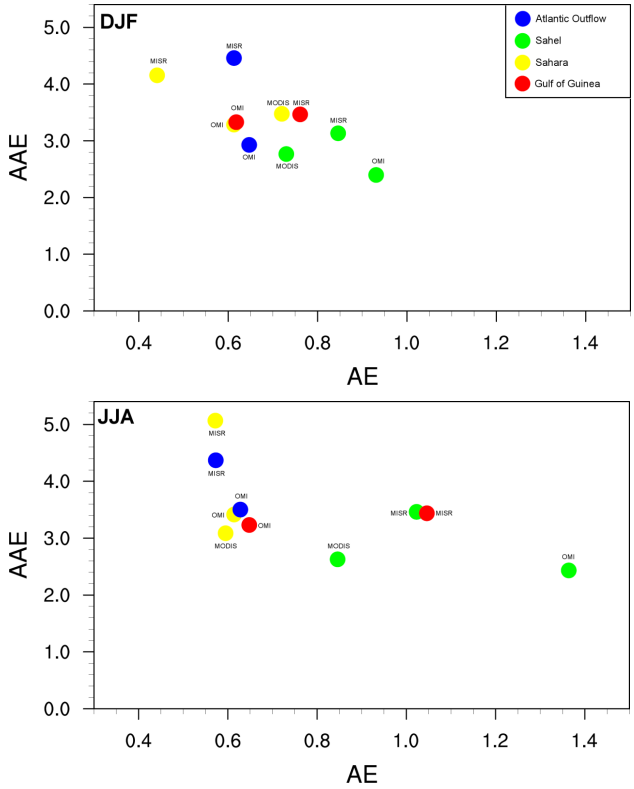

Fig. 5. Scatterplot of Absorption AOT Angstrom exponent (AAE) versus AOT Angstrom exponent (AE) computed using Eq. (1) for **(a)** DJF and **(b)** JJA. The values represent the average over the subdomains represented in Fig. 2.

ACPD
11, 28587–28626, 2011